3556 *Macromolecules* **2010**, *43*, 3556–3565
DOI: 10.1021/ma100093b

Macromolecules
ARTICLE

Mechanism of Shear Thickening in Reversibly Cross-Linked Supramolecular Polymer Networks

Donghua Xu, Jennifer L. Hawk, David M. Loveless, Sung Lan Jeon, and Stephen L. Craig*

Department of Chemistry and Center for Biologically Inspired Materials and Material Systems, Duke University, Durham, North Carolina 27708-0346

Received January 14, 2010; Revised Manuscript Received March 5, 2010

ABSTRACT: We report here the nonlinear rheological properties of metallo-supramolecular networks formed by the reversible cross-linking of semidilute unentangled solutions of poly(4-vinylpyridine) (PVP) in dimethyl sulfoxide (DMSO). The reversible cross-linkers are bis-Pd(II) or bis-Pt(II) complexes that coordinate to the pyridine functional groups on the PVP. Under steady shear, shear thickening is observed above a critical shear rate, and critical shear rate is experimentally correlated with the lifetime of the metal−ligand bond. The onset and magnitude of the shear thickening depend on the amount of cross-linkers added. In contrast to the behavior observed in most transient networks, the time scale of network relaxation is found to increase during shear thickening. The primary mechanism of shear thickening is ascribed to the shear-induced transformation of intrachain cross-linking to interchain cross-linking, rather than nonlinear high tension along polymer chains that are stretched beyond the Gaussian range.

Introduction

The sophistication with which intermolecular interactions can now be rationally engineered has had a major impact on a myriad of fields, including molecular recognition, self-assembly, nanotechnology, and polymer science.[1,2] It has long been appreciated that intermolecular forces between polymer chains contribute to their macroscopic mechanical properties and rheological behavior.[3,4] Recently, the incorporation of highly specific, stoichiometric, and well-characterized associating units as defining interactions in polymers (often referred to as "supramolecular polymers") has attracted much interest.[5] The potential advantages of supramolecular polymers relative to their covalent counterparts include opportunities for new, noncovalent approaches to polymer synthesis,[6,7] the rational control of polymer properties, including stimuli responsiveness,[8,9] and new strategies by which to construct self-repairing materials.[10]

In many cases, the fundamental difference between supramolecular and covalent polymers is the reversibility (kinetic lability) of the supramolecular bond. Yount et al.[11,12] recently demonstrated a conceptually simple, but practically useful, method for probing the contributions of molecular reversibility to the rheological properties of polymers. The methodology takes advantage of steric effects at the *N*-alkyl positions of van Koten's *N*,*C*,*N*-pincer Pd(II) and Pt(II) complexes[13] to change the rates of ligand exchange independently of the association constant. This methodology has been applied in our lab[14] to explore the molecular mechanisms underlying the basic rheological properties of linear supramolecular polymer solutions,[11] supramolecular polymers networks,[12,15] and tribological properties of cross-linked polymer brushes.[16] While the viscosities of solutions of linear supramolecular polymers formed from these metal−ligand interactions depend on the equilibrium constant (K_{eq}) of the metal−ligand interaction,[11] the low-strain, frequency-dependent dynamic moduli of macroscopic polymer networks that are cross-linked via these same interactions (e.g., Figure 1) are related quantitatively to the pyridine exchange rates (k_d) measured on model Pd(II) and Pt(II) complexes.[12,15] These studies are just a part of increasing amount of research regarding the rheological properties of supramolecular polymers[17−24] and their relationship to the nature of the defining supramolecular interactions.

In contrast to their linear rheological properties, the mechanisms underlying the nonlinear rheological properties of supramolecular polymer networks (e.g., strain hardening and shear thickening) are often unclear and have received less attention. (A more involved discussion of shear thickening mechanisms in associative polymer networks is provided in the Discussion section.) In this paper, we extend the methodology of Yount et al.[11,12] to explore the shear thickening properties of metallo-supramolecular networks formed from the addition of bis-Pd(II) or bis-Pt(II) cross-linkers to semidilute unentangled solutions of PVP in DMSO.

Experimental Section

Materials. Dimethyl sulfoxide (DMSO) and poly(4-vinylpyridine) (PVP), M_w = 60 000, were used as received from Aldrich. Four cross-linkers, [2,3,5,6-tetrakis{(dimethylamino)methy}-phenylene-1,4-bis(palladium trifluoromethanesulfonate)] (**1**), [2,3,5,6-tetrakis{(diethylamino)methy}phenylene-1,4-bis(palladiumtrifluoromethanesulfonate)] (**2**), [2,3,5,6-tetrakis{(dimethylamino)methy}phenylene-1,4-bis(platinumtrifluoromethanesulfonate)] (**3**), and [2,3,5,6-tetrakis{(diethylamino)methy}-phenylene-1,4-bis(platinumtrifluoromethanesulfonate)] (**4**), were synthesized as reported elsewhere.[25] The reversible coordinative cross-linkers formed between PVP and bis-functional metal compounds are shown in Figure 2.

Sample Preparation. Samples were prepared as follows. PVP was added to DMSO, stirred for 4 h, and then transferred to vials. Separate solutions of cross-linkers were formed by dissolving them in DMSO. These solutions were then added to the vials containing the PVP/DMSO solution. Samples with different molar ratios of cross-linkers to pyridine units in PVP were prepared, and the molar ratios reported here are those between palladium or platinum atoms (two per cross-linker) and pyridine

*Corresponding author. E-mail: stephen.craig@duke.edu.

 Published on Web 03/17/2010

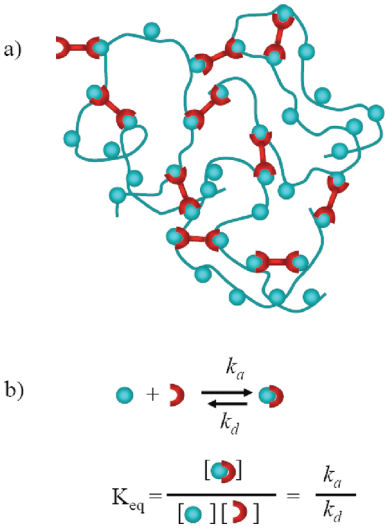

Figure 1. (a) Schematic of a supramolecular polymer network in which polymer side chains are cross-linked by bis-functional recognition units. (b) Thermodynamic and kinetic parameters of the supramolecular interaction underlying network formation.

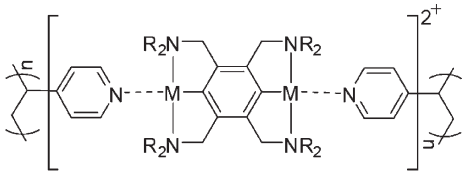

1 M= Pd R= Me

2 M= Pd R= Et

3 M= Pt R= Me

4 M= Pt R= Et

Figure 2. Schematic picture of networks formed from PVP chains and cross-linking bimetallic compounds (**1**−**4**). Two counterions $2[CF_3SO_3]^{1-}$ are not shown in the schematic picture.

nitrogens in PVP.[20] For 60 kDa, there are about 570 pyridine units in each PVP chain (for purposes of this analysis, we assume M_n is equal to the M_w provided by the supplier; the polydispersity of the PVP is not known). At different molar ratios between palladium (or platinum atoms) and pyridine nitrogens (0.5%, 1%, 2%, 3%, 5%, and 7% in this paper), there are about 3, 6, 11, 17, 28, and 40 palladium (or platinum) atoms per PVP chain and half that number of bivalent cross-linkers. Additional DMSO was added to the above vials to adjust the mass concentration of PVP. The prepared samples were then stirred for 12 h at ∼90 °C and subsequently allowed to cool to room temperature. Two different series of samples were prepared, in which the mass concentration of PVP was held roughly constant at ∼0.08 and ∼0.1 g/mL. These concentrations of PVP fall within the semidilute unentangled regime (Figure S1 in the Supporting Information). DMSO is close to a θ solvent for PVP at 25 °C (Supporting Information).

The micromorphology of the samples was checked for phase separation using a phase contrast microscope (Zeiss Axio Observer, Germany). Over sufficiently long times (∼2 h), phase separation was observed in some samples. Phase separation, as observed by microscopy, was faster for samples that were not covered with a cover glass. In addition, we observe no phase separation over a period of more than 6 months (and counting at the time this article was submitted) for samples left in sealed vials. We therefore infer that the phase separation is due to exposure to moist air and that it does not reflect an inherent instability in the samples. All rheological data reported here were obtained under conditions (experimental time scales of 1 h or less) in which no evidence for phase separation was observed.

Table 1. Equilibrium Constants and Dissociation Rate Constants for Pincer Pd and Pt Complexes (1−4) with Pyridine in DMSO at 25 °C [Uncertainties: K_{eq} (20%), k_d (15%)][12]

complex	K_{eq} (M^{-1})	k_d (s^{-1})
1·pyridine	29	1450
2·pyridine	33	17
3·pyridine	8000	0.026
4·pyridine	4000	0.0006

Rheological Measurements. All rheological data were obtained by using an AR G2 rheometer (TA Instruments) with cone−plate geometry (diameter of 20 mm, cone angle of 2°, truncation height of 49 μm). A solvent trap was used with this geometry to minimize the evaporation of solvent from the samples.

The samples were loaded into the plate at 25 °C and heated to 80 °C for 2 min to erase the thermal and mechanical history. The samples were then compressed to a height of 55 μm, excess material was scraped from the edge of the geometry, and the samples were cooled to 25 °C. Next, the samples were compressed to 49 μm (the truncation height of the geometry), and the experiment was started. Experiments were carried out at 25 °C (unless otherwise noted). The stiffness of samples with high concentrations of bis-Pt(II) cross-linkers precluded proper loading, and as a result rheological experiments for those samples were not performed.

Strain sweep experiments were performed at a frequency of 10 rad/s (unless otherwise noted) to determine the region of linear response. Oscillatory frequency sweeps from 0.1 to 500 rad/s were carried out with an appropriate strain within the linear region. Steady shear measurements typically were performed over a range of shear rates between 10^{-3} and 10^3 s^{-1}, although higher shear rates were occasionally employed for samples with low viscosity.

Parallel superposition of oscillation onto steady-shear flow was carried out at various applied stresses to determine the change of the relaxation time of the samples under different stress. A detailed introduction to the superposition technique can be found in an earlier report by Tam et al.[26]

Results

Three States of Cross-Linkers in the Samples. The binding thermodynamics and exchange kinetics of the metal−pyridine interactions have been characterized previously.[12,15] The previously reported equilibrium association constants (K_{eq}) and dissociation rate constants (k_d) are summarized for convenience in Table 1.

In our samples, the cross-linkers might take any of three different states, which we denote here as free, dangling, and bound states. The bound state is the state in which each of the two metal centers in the bis-Pd(II) (or bis-Pt(II)) cross-linkers is coordinated to a pyridine unit along the PVP. Of critical importance is the fact that the bound state may exist as either an interchain or an intrachain cross-linker. While intrachain bonds neither contribute to the formation of the network nor act as "elastically active chains",[27] interchain bonds are critical for gelation and contribute to the network modulus. By the dangling state, we refer to a bis-Pd(II) (or bis-Pt(II)) cross-linkers that is bound to a PVP pyridine unit only on one end. The third state, that of the free bis-Pd(II) (or bis-Pt(II)) cross-linkers, is that in which neither metal center is coordinated to a pyridine unit.

Because the Pd−pyridine (or Pt−pyridine) coordination bond is labile, each bis-Pd(II) (or bis-Pt(II)) complex constantly changes between the three states. The distribution of states among all bis-Pd(II) (or bis-Pt(II)) complexes, however, achieves (pseudo)equilibrium or steady-state values.

Using the equation as shown in Figure 1b and accounting for the presence of two binding sites on our cross-linkers, the fractions of free (p_f), dangling (p_d), and bound (p_b) cross-linkers can be derived:

$$p_f = \frac{1}{K_{eq}^2[A]_{eq}^2 + 2K_{eq}[A]_{eq} + 1} \quad (1)$$

$$p_d = \frac{2K_{eq}[A]_{eq}}{K_{eq}^2[A]_{eq}^2 + 2K_{eq}[A]_{eq} + 1} \quad (2)$$

$$p_b = \frac{K_{eq}^2[A]_{eq}^2}{K_{eq}^2[A]_{eq}^2 + 2K_{eq}[A]_{eq} + 1} \quad (3)$$

where $[A]_{eq}$ is the concentration of pyridine unit at equilibrium state. The fraction of different states of cross-linkers in an equilibrium state depends on K_{eq}, the initial concentration of PVP, and the initial concentration of cross-linkers. In our experiments, p_b for bis-Pd(II) is about 0.91−0.94 and p_b for bis-Pt(II) is about ∼0.999; p_d for bis-Pd(II) is about 0.056−0.086 and p_d for bis-Pt(II) is about $\sim 10^{-4}$; and p_f for bis-Pd(II) is about $\sim 10^{-3}$ and p_f for bis-Pt(II) is about $\sim 10^{-7}$. (The calculations responsible for these values are described in greater detail in the Supporting Information.) The overwhelming majority of the bis-Pd(II) (or bis-Pt(II)) cross-linkers, therefore, are expected to be in the bound state in our samples, and the average ratio of bound state cross-linkers to PVP chain ranges from ∼1:1 to 20:1 across the concentration ranges studied here.

Linear Rheological Properties. The linear rheology of similar cross-linked PVP networks has been explored previously in some detail by our group.[12,15] Nevertheless, the specific concentrations and conditions employed here are slightly different from those in previous studies, and so we began by confirming the linear rheology of these samples. The storage (G') and loss (G'') moduli for ∼0.1 g/mL PVP with different concentrations of **2** are shown as a function of frequency in Figure 3. The modulus of ∼0.1 g/mL PVP with 0.5% **2** is small and outside of the measurement range of the rheometer. As the concentration of **2** increases from 1% to 7%, both the storage and loss moduli increase more than 3 orders of magnitude. At these higher concentrations of **2**, the bulk relaxation rate (β) of the networks can be obtained from the crossover points between G' and G''. The plateau moduli (G_0) are obtained from the high-frequency measurements.

As expected based on previous reports on the same systems at different concentrations,[12,15] the storage and loss moduli curves are shifted to higher frequencies when the faster bis-Pd(II) cross-linker **1** is used in place of **2**. Also as previously reported, the dynamic mechanical properties of the PVP·**1** and PVP·**2** networks are superposed onto a single master curve by scaling the frequency of the oscillatory experiment by k_d measured for model Pd−pyridine complexes, consistent with the expectation that the Pd−pyridine interactions define the elastically active segments in the network. While the crossover points of G' and G'' for the PVP·**1** networks are not observed within the experimental range accessible on our rheometer, they can be inferred through the scaling relationship. In Figure 4, superposition of G' and G'' versus scaled frequency for ∼0.1 g/mL PVP with **1** or **2** (above 1%) is shown. We note that the data for the network formed from ∼0.1 g/mL PVP with 1% **1** cannot be superposed with that formed from 1% of **2**, consistent with previous observations regarding cross-linker concentrations that are near the gel point.[19]

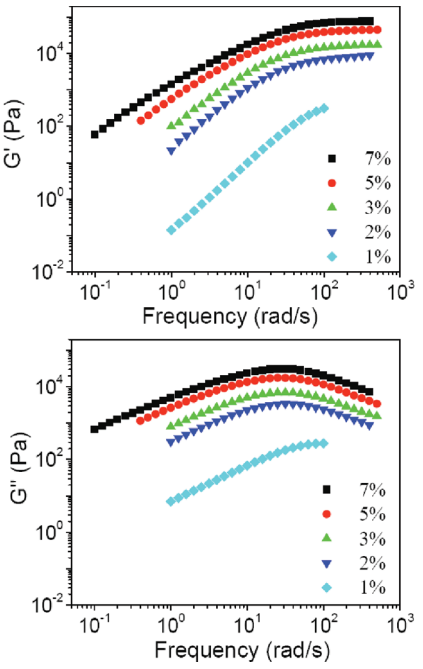

Figure 3. Storage modulus (G') and loss modulus (G'') versus frequency for ∼0.1 g/mL PVP with different concentrations of **2**. Concentration of cross-linkers means molar ratio between Pd:N here and below unless otherwise noted.

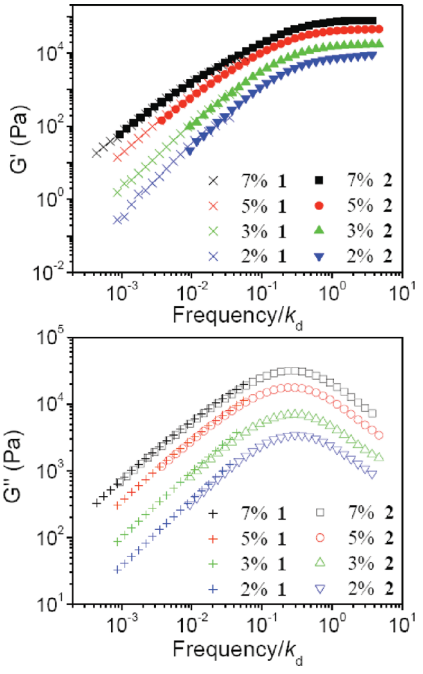

Figure 4. Storage modulus (G') and loss modulus (G'') versus scaled frequency for ∼0.1 g/mL PVP with different concentrations of **1** or **2**.

The slopes of G' and G'' in the terminal zone for 0.1 g/mL PVP with **2** showed unusual terminal behavior with power-law dependencies for G' and G'' versus frequency (ω) having much smaller slopes than those expected of a single-element Maxwell model: $G' \sim \omega^2$ and $G'' \sim \omega^1$, respectively. With the increasing concentration of **2** from 1% to 7%, the power-law dependencies for G' versus ω range from 1.86 to 1.33; the power-law dependencies for G'' versus ω range from 0.98 to

0.85. This behavior has also been noted previously,[12,28] and it is apparent that the relaxation modes in these samples are more complex than can be described by the single apparent relaxation time obtained by the crossover of G' and G''.

Shear Thickening. Steady shear viscosity versus shear rate for ~0.1 g/mL PVP with **1** or **2** is shown in Figure 5. Zero-shear viscosity of ~0.1 g/mL PVP with 0.5% **1** or **2** is just a little higher than the pure ~0.1 g/mL PVP solution (0.021 Pa·s). This indicates that the concentration of 0.5% cross-linker is below the gel concentration for the formation of network. With the increasing of concentration of cross-linker above 1%, the viscosities of the two mixtures are significantly different (and scale with the difference between the dissociation rates of **1** and **2**). This is consistent with the previous results in our group that the gel concentration of cross-linkers for forming network is ~0.8%.[12,19] For samples with concentration of cross-linker above the gel concentration, the steady shear viscosity exhibits three flow regimes with the increasing of shear rate, which are Newtonian, shear thickening, and shear thinning. The steep decrease in viscosity at high shear rates (Figure 5) is attributed to network fracture[29] and/or the subsequent ejection of sample from the rheometer geometry (one video as an example in the Supporting Information). Strain hardening is also observed for those samples which show shear thickening. The strain hardening behavior of these networks is currently under investigation and it is not explored further here.

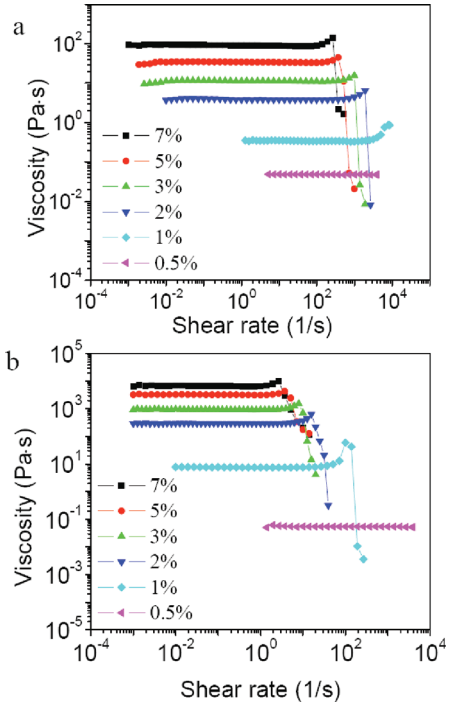

Figure 5. Steady shear viscosity versus shear rate for ~0.1 g/mL PVP with different concentrations of **1** (a) and **2** (b).

Table 2 shows a comparison of compiled parameters (from Figure 3–5) for the ~0.1 g/mL PVP solution with **1** or **2**. From Table 2, we can get the Weissenberg number (shear rate divided by relaxation rate, $\dot{\gamma}/\beta$) at the lowest shear rate at which thickening is observed ($\dot{\gamma}_{start}$) and the shear rate at which the viscosity reaches its maximum point ($\dot{\gamma}_{max}$). In polymer solutions, a Weissenberg number that is larger than 1 corresponds to orientation of polymer chains.[3] For ~0.1 g/mL PVP solution with 1% **2** at $\dot{\gamma}_{start}$, the Weissenberg number is about 1.4. With the increasing of concentration of **1** or **2** (above 1%), the Weissenberg number ranges from 0.3 to 0.76 at the shear thickening start point. The onset of shear thickening at Weissenberg numbers that are less than 1 might be due to the wide distribution of relaxation times of our samples (see above), but the correlation supports the assertion that the shear thickening in our samples is connected with the orientation of polymer chains.

As seen in Table 2, the ratio between the maximum viscosity at the shear thickening peak and the zero shear viscosity during shear thickening (η_{max}/η_0) ranges from 1.3 to 5.9. The degree of shear thickening here is in the same range as reported for hydrophobically modified urethane–ethoxylate (HEUR) or hydrophobically modified alkali-soluble emulsion (HASE) associative polymer solutions under different conditions.[30–34] These and other parameters in Table 2 are discussed in more detail below.

Discussion

Shear Thickening of Associative Polymers. The molecular origin of shear thickening has been debated over the past two decades on the basis of experimental[26,35,36] and theoretical[36–39] evidence. To date, the mechanisms for shear thickening of associative polymers have been classified into two main categories. The first ascribes thickening to the nonlinear high tension along stretched polymer chains beyond the Gaussian range,[30,31,38] while the second attributes thickening to an increase in the number of elastically active chains.[26,40–42]

An example of the latter, a "structure-forming" mechanism is found in the work of Witten et al., who sketched a picture of shear thickening in which the flow produces increased association between chains at the expense of associations within a chain.[42] Witten's theory was doubted by Wang, who argued that when the lifetime of the association is much longer than the relaxation time of free chains,

Table 2. Parameters for ~0.1 g/mL PVP Solution with 1 and 2 (From Oscillatory Frequency Sweep and Steady Shear Experiment)[a]

samples	β (s^{-1})	$\dot{\gamma}_{start}$ (s^{-1})	$\dot{\gamma}_{start}/k_d$	$\dot{\gamma}_{max}$ (s^{-1})	$\dot{\gamma}_{max}/k_d$	σ_{max} (Pa)	η_{max}/η_0
7% **1**	243.1	71.97	0.04963	268.3	0.185	38330	1.5
5% **1**	252.5	100	0.06897	372.8	0.2571	16740	1.3
3% **1**	302.8	193.1	0.1332	1000	0.6897	15540	1.4
2% **1**	355.7	268.3	0.185	1931	1.332	12460	1.7
1% **1**		1585	1.093	7944	5.478	6937	2.6
7% **2**	2.85	1	0.05882	2.686	0.158	27250	1.4
5% **2**	2.96	1.389	0.08171	3.727	0.2192	16380	1.3
3% **2**	3.55	2.512	0.1478	7.944	0.4673	12400	1.6
2% **2**	4.17	3.162	0.186	15.85	0.9324	10200	2.1
1% **2**	13.92	19.31	1.136	100	5.882	3344	5.9

[a] β (s^{-1}) is the relaxation rate of samples. $\dot{\gamma}_{start}$ (s^{-1}) is the shear rate where the steady-shear viscosity starts to increase at the beginning of shear thickening. $\dot{\gamma}_{max}$ (s^{-1}) is the shear rate where the steady-shear viscosity reaches maximum viscosity during shear thickening. $\dot{\gamma}_{start}/k_d$ and $\dot{\gamma}_{max}/k_d$ are the scaled value of $\dot{\gamma}_{start}$ and $\dot{\gamma}_{max}$, respectively. σ_{max} is the shear stress where the steady-shear viscosity reaches maximum viscosity during shear thickening. η_0 is the zero shear viscosity. η_{max} is the maximum viscosity during shear thickening. η_{max}/η_0 represents the degree of shear thickening.

flow cannot break strong intrachain associations until most interchain associations are broken.[41] Wang subsequently introduced free chains into a transient network model and predicted that shear thickening is the result of coagulation of free chains into the existing network.[41]

In contrast, Marrucci et al.[38] attributed shear thickening to a non-Gaussian chain stretching effect within a network whose number of elastically active chains does not change during shear. Within the basis of a transient network model, they replaced the linear force law describing chain extension with an inverse Langevin function and found shear thickening as a result of non-Gaussian chain stretching, although the magnitude of shear thickening predicted by this theory was smaller than that observed experimentally. Marrucci et al. further assumed that a polymer chain can only partially relax its extended conformation when the chain end dissociates from a network junction (the free path model). In the free path model, the critical shear rate is estimated by assuming that the elastically active chains reach full extension at the onset of shear thickening.[38] Under these assumptions, the shear rate at maximum viscosity ($\dot{\gamma}_{max}$) is approximately

$$\dot{\gamma}_{max} \approx N^{1/2}/\tau \tag{4}$$

where N is the number of Kuhn segments in the chain and τ is the network relaxation time. The critical shear stress at the shear thickening maximum point (σ_{max}) is estimated to be

$$\sigma_{max} \approx \nu k_B T N^{1/2} \tag{5}$$

where ν is the number of elastically active chains, k_B is Boltzmann's constant, and T is the temperature. According to eq 5, the σ_{max} is found to be independent of τ and depends only on chain molecular weight and concentration. The free path model predicts that the viscosity attains a maximum value given by

$$\eta_{max} \approx \nu E_a \tau = (E_a/k_B T)\eta_0 \tag{6}$$

where E_a is the activation energy of the association. Thus, the value of the viscosity maximum depends directly on the energy barrier $E_a/k_B T$. Subsequent work showed good agreement with the prediction of the free path model for critical shear rate, critical shear stress, and the magnitude of shear thickening.[30]

Recently, Tripathi et al. proposed a modified nonlinear constitutive model for telechelic associative polymers.[33] The model incorporates contributions to the total stress tensor from both the "elastically active" bridging chains between micelles and the dangling chains that continuously exit and reenter the micellar junctions. Nonlinear chain extension, the shear-induced enhancement of associations, and the stretch-induced dissociation of hydrophobic chains are essential features of the model. Tripathi et al. then compared the model predictions with a systematic experimental study of the linear viscoelastic, steady shear, and transient extensional properties of a series of well-characterized model hydrophobically modified ethoxylate−urethane (HEUR) polymers possessing varying degrees of hydrophobicity. All experimental results such as shear thickening at intermediate shear rate followed by shear thinning at higher shear rate (or only shear thinning for some higher concentration samples) can be fit very well by the above model by changing a single dimensionless constitutive parameter G_m, which describes the orientational and deformation-rate-dependent creation rate of the active chains. G_m is given by

$$G_m = \tau_s/\tau_E \tag{7}$$

where τ_s is the characteristic interaction time of hydrophobic ends with the surrounding fluid medium comprising a lattice of attractive micelles and τ_E is exit time of the hydrophobic ends. For samples showing shear thinning, G_m is expected to be less than 1. For samples show shear thickening, G_m is expected to be larger than 1.[33] While τ_E has the clear meaning as lifetime of reversible bond ($1/k_d$ in our experiment), the analogous definition for τ_s (or a similar parameter) is not clear in our experiments.

Inherent Ambiguity between the Non-Gaussian Stretching and Structural Reorganization Mechanisms. The initial question regarding the mechanism of shear thickening observed in our samples, therefore, is whether it involves non-Gaussian stretching of active chain segments within an effectively intact network structure or whether the cross-linkers within the transient network actually reorganize into a new structure in response to the applied shear. Such distinctions are typically challenging to realize, for reasons that we now discuss. Consider the behavior of the coordinative PVP networks (Figures 4 and 5) and the fact that the onset of shear thickening during steady shear is well-correlated with the relaxation rate of the network (Table 2), which in turn reflects the kinetics of metal−ligand dissociation in the defining cross-linking coordination bonds. This observation strongly implies a requirement for chain orientation within active chain segments, since the opportunity for relaxation of the network (through dissociation of the metal−ligand bond) inhibits the shear thickening. The presence of chain orientation is further supported by the relationship between the onset of shear thickening and the Weissenberg number, as described previously. The fundamental difficulty lies in the fact that both structural reorganization and non-Gaussian overstretching involve chain orientation under applied shear, and so both mechanisms by necessity will have many dynamic experimental signatures in common.

For example, the free path model described above, which is one example of non-Gaussian stretching within an effectively static network, can be applied to our observations with some qualitative success: as noted above, the onset of shear thickening as a function of shear rate scales with the metal−ligand dissociation rate, and this is predicted by eq 4 . In addition, the critical shear stress at the shear thickening maximum point (σ_{max} in Table 2) is almost the same and independent of the differences in the kinetics of cross-link dissociation rate for **1** and **2**, as expected from eq 5. But similar scaling behaviors should, in general, be observed as a function of network reorganization as well, under which circumstances the ultimate network responses for **1** and **2** are expected to be identical except for the time scale on which they occur. Thus, consistency with the free path model is not direct proof that shear thickening is caused by non-Gaussian stretching.

Evidence of a Shear-Induced Increase in the Number of Elastically Active Chains. One distinguishing feature between the reorganization and overstretching models involves the expected influence of each on network relaxation time.[33] In Marrucci et al.'s work,[38] the relaxation time of the network is calculated to be

$$\tau \approx \frac{Nb^2}{a^2}\beta_0^{-1} \tag{8}$$

where a is the average spatial distance among neighboring aggregates (cross-linkers), N is the number of Kuhn chain

segments in the polymer chain, b is the Kuhn length, and β_0 is the chain detachment rate under equilibrium conditions (k_d in our formalism). In Marrucci et al.'s work, a is related to the number of elastically active chains (ν) as[38]

$$\nu a^3 = 1 \tag{9}$$

Tripathi's work results in a similar equation:[33]

$$\tau \sim \frac{Nb^2/3}{\langle a \rangle^2}\tau_E \tag{10}$$

In the case of an intact network in which shear thickening occurs as a result of non-Gaussian stretching, τ generally remains constant in the linear regime and decrease during the shear thickening phenomenon.[31] Under this mechanism, the decrease of τ may result in the increase of a during stretching of polymer chain or the decrease of ν when the elastic energy of polymer chain compares with the activation barrier for cross-linkers.[31] τ might also decrease because dissociation rate is accelerated by a coupled force.[43] On the other hand, if shear thickening results from an increase in the number of elastically active chains, a decrease in a is expected, which should in turn lead to an increase in the measured relaxation time of the network. Characterizing the change (or lack thereof) of τ during shear thickening, therefore, provides strong evidence for the mechanism underlying shear thickening.

We determine the relaxation time of the samples under different stress through parallel superposition of oscillation on steady-shear flows (strain rate tensor applied by oscillation in the direction of velocity).[26] It is important to note the limitations of the parallel superposition technique, in particular when used to characterize the absolute value of moduli. For example, the moduli obtained by parallel superposition cannot be treated as linear viscoelastic moduli, and in fact, apparently negative moduli have been obtained at low frequency; orthogonal superposition (strain rate tensor applied by oscillation in the direction of vorticity) is thought to be a better way to characterize the modulus.[32] On the other hand, parallel superposition is still a sensitive method by which to obtain trends in the change of relaxation time within the sheared network. For example, Mewis et al. have reported that both parallel and orthogonal superposition give the same trends for network relaxation time as a function of applied shear stress for a poly(isobutene)/decalin solution and a hydrophobic alkali-swellable emulsion (HASE), even though the values of the relaxation times obtained by the two methods differ, especially in the nonlinear regime.[32,44] At the same time, Tam et al.[45] and Mewis et al.[32] both reported that the relaxation time of a shear thinning HASE associative polymer decreases with increasing shear stress.[31,45] Munoz et al. researched shear thickening in glyerine solutions of poly-(2-hydroxyethyl methacrylamide) and found that the relaxation time does not change when the applied shear stress lies inside the limits of the linear regime but increases with the applied shear flow for values of the shear stress associated with shear thickening. This observation is attributed to the shear-induced formation of hydrogen bonds.[46] This prior work justifies parallel superposition as a reliable method for characterizing the dependence of relaxation time on an applied shear stress.

Results are shown in Figure 6 for four networks of PVP with concentrations of cross-linker **2** ranging from 2 to 7% (average ratio of bound cross-linkers to number of PVP chains ranges from ~5 to 20). In all cases, the maximum applied shear stress is less than the critical shear stress defined by the shear thickening maximum point, ensuring that the network is not broken during the parallel superposition experiment. In Figure 6, shear stresses less than $\sim 10^3$ Pa correspond to the linear viscoelastic regime observed in the steady shear experiments, and the relaxation times τ derived from the parallel superposition in this regime are close to those obtained from the network relaxation time under dynamic oscillatory stress without superposition (Table 2). In addition, τ is effectively independent of shear stress for shear stresses less than $\sim 10^3$ Pa.

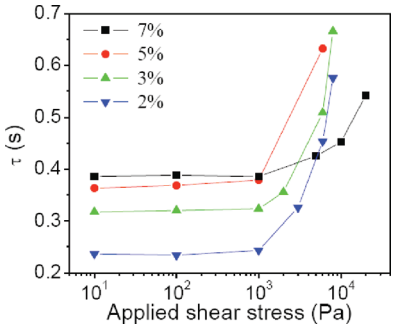

Figure 6. Plot of relaxation time (τ) of ~0.1 g/mL PVP solution with different concentration of **2** versus applied shear stress imposed during parallel superposition of oscillation on steady-shear flow measurements.

The onset of shear thickening occurs at shear stresses of $\sim 10^3$ Pa, and above this threshold value we observe an increase in τ with increasing shear stress. The increased relaxation time is not typical for transient networks, and it is observed here at all concentrations of cross-linker. As discussed above, we regard only the direction of the change in τ with increasing shear stress as reliable, rather than the absolute value of τ in the nonlinear regime. In 0.1 g/mL PVP with 2% **2**, for example, τ changes from ~0.23 to ~0.55 s as the applied shear increases. From eqs 8 and 9, τ scales with ν as $\tau \sim \nu^{2/3}$. If the increase in τ derives entirely from an increasing number of elastically active chains, ν would increase by a factor of 2.8 with the increased shear. As discussed below, this increase is larger than can reasonably be expected (see, e.g., Figure 9 and related discussion). We infer that the exact value of τ in the shear thickening regime should be lower than the apparent value shown in Figure 6.

As described above and seen empirically in the low-stress regime of Figure 6, the increased relaxation time is consistent with an increased density of active cross-linkers and contradicts the behavior expected from non-Gaussian overstretching in an effectively intact network. While shear thickening of the bis-Pd(II)−PVP networks is not dominated by non-Gaussian overstretching, however, the presence of structural reorganization need not preclude contributions from non-Gaussian effects.

Evidence of Non-Gaussian Stretching of Polymer Chains during Steady Shear. As a polymer chain is stretched under shear, the stress along the polymer chain will increase exponentially with the strain.[47] When the elastic energy of the polymer chain is comparable to the dissociation energy of the cross-linker, the supramolecular polymer network will break. The break of such a supramolecular polymer network was experimentally observed by Séréro et al., who researched the rheology and microstructure of aqueous solutions of telechelic polymers with a poly(ethylene oxide) middle block and semiperfluorinated end-caps. Those authors referred to the process as fluid fracture.[29] A sharp decrease in viscosity after shear thickening (called fluid fracture in their paper) was observed, similar to what we report here.[29,31] Séréro et al.

conclude that above the linear regime the active chains are stretched in the non-Gaussian range of extensions, and consequently, the network hardens due to the increase of the entropic restoring forces. For rates and stresses large enough, there is a catastrophic breakdown or rupture of the network leading to a low-viscosity flow. Similar behavior is observed here, and so we infer that non-Gaussian stretching of polymer chains in our samples does take place, especially during the rupture of network (shear thinning regime during steady shear). While network fracture clearly occurs, however, the shear thinning behavior cannot be attributed to network fracture alone, as the shear thinning behavior here correlates with the ejection of sample from the rheometer geometry.

We note that while forced dissociation of the cross-links and fluid fracture could, in theory, occur at forces below those associated with non-Gaussian stretching, it is unlikely. Vaccaro et al. have estimated the elastic energy of a polymer chain needed to pull off cross-linkers.[48] As long as the chain remains Gaussian, the elastic tension F in the chain grows proportionally with the end-to-end distance R according to[48]

$$F(R) = \frac{3k_BT}{Nb^2}R \tag{11}$$

where b and N are the length and number of the chain Kuhn segments, respectively. In the linear region, R remains much smaller than the fully extended chain length Nb, and the tension F remains well under k_BT/b, or on the order of several piconewtons. Previous force spectroscopy work in our group has shown that more than 50 pN of force is required to accelerate the rate of cross-link dissociation by a factor of 10, and so the forces associated with stretching of the polymer chains in the linear regime are not sufficient to explain the catastrophic fracture observed at high shear rates.[43] These arguments strongly suggest that high shear rates do eventually lead to non-Gaussian stretching of active polymer chain segments within the network.

Molecular Mechanism Underlying Shear Thickening in Our Samples. One method to determine the relative contributions of these two shear thickening mechanisms is to compare the extent of shear thickening with theoretical expectations. According to the free path model, shear thickening from non-Gaussian overstretching leads to a maximum increase in viscosity η_{max} which is proportional to the zero-shear viscosity η_0 through the activation energy for bond dissociation (eq 6).[38] In our experiments, the free energies of activation (ΔG) of the four cross-linkers are calculated by the Eyring equation:[49]

$$k_d = 2.083 \times 10^{10} T e^{-\Delta G/RT} \tag{12}$$

where R is the gas constant. In our experiments, ΔG of the four cross-linkers at 25 °C are 55, 66, 82, and 91 kJ/mol for **1** through **4**, respectively. The internal energies of activation (E_a) of the four cross-linkers are also calculated to be 42, 53, 64, and 74 kJ/mol for **1** through **4**, respectively (see Supporting Information). As seen in Figure 7, however, it is apparent that η_{max}/η_0 does not increase with the increasing ΔG (or E_a) of the four cross-linkers, in contrast to Marrucci's free path model. This is consistent with a picture in which non-Gaussian overstretching of polymer chains has a weak influence on shear thickening.

In Figure 7, we notice that η_{max}/η_0 of 0.08 g/mL PVP solution with 1% of cross-linkers varies substantially from one cross-linker to another. Because a cross-linker concentration of 1% is near the gel point (~0.8%),[19] η_{max}/η_0 here is expected to be quite sensitive to the precise concentration

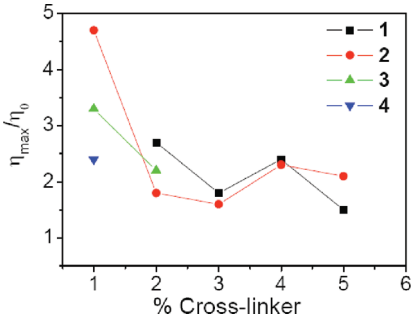

Figure 7. Degree of shear thickening (η_{max}/η_0) of ~0.08 g/mL PVP solution with four different cross-linkers (**1**−**4**) versus the concentration of cross-linkers is shown.

of cross-linkers. We therefore attribute the variations in η_{max}/η_0 of 0.08 g/mL PVP solution with 1% cross-linkers to small differences in the concentration of cross-linkers during preparation of samples. On the other hand, η_{max}/η_0 of 0.08 g/mL PVP solution with higher concentrations of cross-linkers remains in the range of 1.5−2.5 (same trends as shown in Table 2 for 0.1 g/mL PVP with **1** or **2**). These data are presented for the sake of completeness only and do not impact the conclusions of this work.

Another approach to elucidating the shear thickening mechanism is through kinetic studies of the shear thickening process. While non-Gaussian stretching of polymer chains occurs on the time scale of chain elongation, the mechanism of shear-induced reorganization requires that cross-linkers must dissociate in order to rearrange to form new network structure. In the latter case, the structural transformation is not instantaneous upon application of sufficient shear stress but requires cross-linker reorganization that occurs on the time scale of $1/k_d$ or longer. The kinetics of shear thickening were investigated using peak hold shear experiments following preshear. A faster sampling rate (1 point per second) was employed during these peak hold shear experiments than in the steady shear experiments (~1 point per minute). The peak hold shear rate was changed to a value within the observed shear-thickening regime. In Figure 8, peak hold shears of three samples are shown as examples. For 0.1 g/mL PVP with 7% of **1** (Figure 8a), the sampling rate of peak hold shear (1 point per second) is too slow to observe the transition, consistent with changes in the network that occur on the time scale of network relaxation through cross-link dissociation (~0.004 s). For 0.1 g/mL PVP with 7% of **2** (Figure 8b), an initial decrease of viscosity at the beginning of peak hold shear is observed, followed by subsequent shear thickening. The kinetics are obviously not those of a smooth, single-step transformation. Again, the time scale of this process is on the order of the relaxation time of this sample (~0.35 s). For 0.08 g/mL PVP with 1% of the much slower cross-linker **3** (relaxation time ~21 s), the steady state under peak hold shear is reached around ~100 s (Figure 8c). Berret et al. performed similar start-up shear experiments on telechelic polymer networks (Figure 4 in ref 35).[35] The steady state is achieved around ~100 s, which is also comparable to the relaxation time of their network (~26 s). In their work, they also show that the rupture of the network caused by non-Gaussian stretching of polymer chain takes place at fixed strain during start-up shear (Figure 8 in ref 35). As the shear rate increases above the critical value so that the stress cannot relax via dissociation of cross-linkers, the rupture of the network accelerates under the increased stress. This strongly suggests that non-Gaussian stretching of elastically active polymer chain segments occurs on shorter time scales

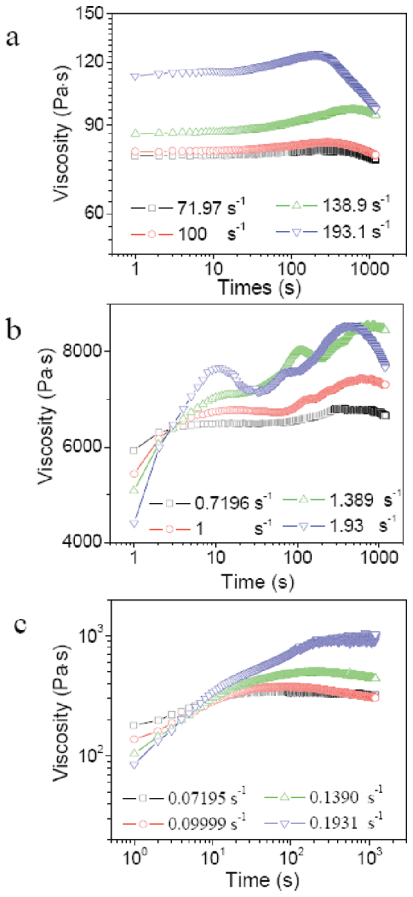

Figure 8. (a) Peak hold shear at different shear rates after preshear from 10^{-3} to 51.79 s^{-1} for ~0.1 g/mL PVP with 7% **1**. (b) Peak hold shear at different shear rates after preshear from 10^{-3} to 0.5179 s^{-1} for ~0.1 g/mL PVP with 7% **2**. (c) Peak hold shear at different shear rates after preshear from 10^{-3} to 0.037 28 s^{-1} for ~0.08 g/mL PVP with 1% **3**.

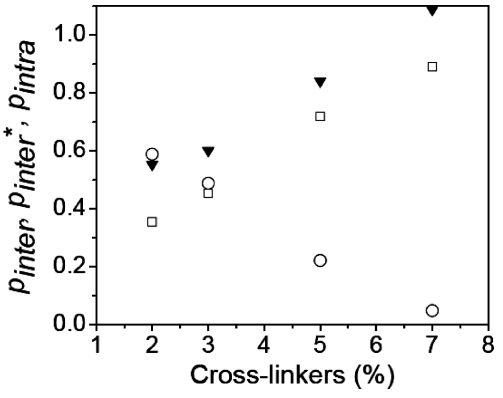

Figure 9. Fraction of interchain bound cross-linkers (p_{inter}) and intrachain bound cross-linkers (p_{intra}) for ~0.1 g/mL PVP solution with different concentrations of cross-linkers **2**: fraction of interchain bound cross-linkers (p_{inter}) at equilibrium state (□); fraction of intrachain bound cross-linkers (p_{intra}) at equilibrium state (○); estimated interchain bound cross-linkers at shear thickening maximum point (p_{inter}*) (▼).

than does the shear induced increase in the number of elastically active chains. We therefore infer that shear thickening in our samples is a two (or more) state process that comprises first partial breakage of the original network structure, followed by orientation of the polymer chains and the subsequent re-formation of a network structure with a higher density of elastically active interchain cross-linking.

Origin of the Shear-Induced Elastically Active Chain Segments. We have concluded that a structural rearrangement within the network underlies the shear thickening behavior, but two possibilities for the molecular origins of this structural transition exist: (i) the increased number of elastically active chains may result from the shear-induced transformation of intramolecular associations to intermolecular associations[40,42] (here, conversion of bound cross-linkers from an intrachain to interchain state), or (ii) the newly active chains may result from shear-induced incorporation of floating chains into the network backbone[41] (conversion from dangling to interchain bound state). To distinguish which effect dominates the shear thickening in our system, we compare the extent of shear thickening and apparent number of shear-induced elastically active chains with estimates of the number of cross-linkers in the intrachain bound and dangling states.

The frequency sweep data provide the plateau modulus G_0, from which the density of elastically active chains (ν) can be calculated[47]

$$G_0 = \nu k_B T \tag{13}$$

In the present work, ν corresponds to the number of interchain bound cross-linkers per unit volume in the 0.1 g/mL PVP solution. The total number of bis-Pd(II) complexes per unit volume (ν_0) is calculated from the concentration of cross-linkers. The ratio ν/ν_0 in the 0.1 g/mL PVP solution is then taken to be the fraction of interchain bound state cross-linkers (p_{inter}), and the fraction of intrachain bound state cross-linkers (p_{intra}) can be calculated from the difference between bound state cross-linkers (p_b) and interchain bound state cross-linkers (p_{inter})

$$p_{intra} = p_b - p_{inter} \tag{14}$$

The values of p_b, p_{inter}, and p_{intra} change with concentration, and Figure 9 shows calculated equilibrium values for each at 0.1 g/mL PVP and varying concentrations of **2**, using eqs 3, 13, and 14. As the density of cross-linkers (ν_0) increases, so too does the fraction of those cross-linkers that form elastically active chains (ν/ν_0 or p_{inter}), which increases smoothly from ~0.35 to ~0.89 as the concentration of cross-linkers increases from 2% to 7%. According to eqs 6, 8, and 9, the scaling law between zero shear viscosity and number of interchain bound cross-linkers is $\eta_0 \sim \nu^{5/3}$.[38] By assuming that the increased viscosity during shear-thickening is attributed entirely to the addition of new cross-linkers and that the same scaling law applies, we therefore infer that p_{inter} increases at the maximum viscosity during shear thickening by a factor of $(\eta_{max}/\eta_0)^{3/5}$ from its zero-shear equilibrium value. From the η_{max}/η_0 data in Table 2, interchain bound cross-linkers at shear thickening maximum point (p_{inter}*) is from 1.2 to 1.6 times larger than p_{inter} at equilibrium state, with apparent maximal values of from 0.55 to 1.09 depending on cross-linker concentration.

These values are clearly only approximate—it is impossible, for example, for p to exceed 1—but they provide a reasonable framework through which to assess the extent of structural reorganization. Table 3 shows the calculated fraction of bis-Pd(II) complexes that become active during shear (from Figure 9) in comparison to the fraction of bis-Pd(II) complexes that are calculated to exist in the free, dangling, and intrachain bound states (from Figure S2 in Supporting Information). The comparisons in Table 3 show that the fraction of free and dangling state cross-linkers is too small for their conversion to active cross-linkers to account

Table 3. Fraction of Cross-Linkers of ~0.1 g/mL PVP with 2[a]

samples	p_f (%)	p_d (%)	p_b (%)	p_{inter} (%)	p_{intra} (%)	p_{inter}* (%)	Δp_{inter} (%)
7% **2**	0.1	6.1	93.8	89.0	4.8	108.9	19.9
5% **2**	0.1	5.9	94.0	71.9	22.1	84.1	12.2
3% **2**	0.1	5.8	94.2	45.4	48.8	60.2	14.8
2% **2**	0.1	5.7	94.2	35.4	58.8	55.3	19.9

[a] p_f is the fraction of free state cross-linkers. p_d is the fraction of dangling state cross-linkers. p_b is the fraction of bound state cross-linkers. p_{inter} is the fraction of interchain bound cross-linkers at equilibrium state. p_{inter}* is the fraction of interchain bound cross-linkers at shear thickening maximum point. p_{intra} is the fraction of intrachain bound cross-linkers at equilibrium state. Δp_{inter} is the difference between p_{inter} and p_{inter}*.

for the full extent of shear thickening. For the data of 0.1 g/mL PVP with 7% of **2**, p_d is larger than p_{intra}. It seems that both dangling state cross-linkers and intrachain bound cross-linkers may transfer to interchain bound cross-linkers. But other examples show that the transfer of p_d to p_{inter} is not necessarily needed to account for the magnitude of shear thickening. For example, ~0.08 g/mL PVP with **3** or **4** has p_d less than ~0.1% while p_b is larger than ~99.9%. From the value of η_{max}/η_0 of them (Figure 9), we can see that the fraction of free and dangling state cross-linkers is far too small for their conversion to active cross-linkers to account for the extent of shear thickening. By comparison, the cross-linkers that are originally in an inactive intrachain bound state are present in sufficient numbers to roughly account for the enhanced viscosity due to shear thickening. We conclude, therefore, that the shear thickening is primarily due to a shear-induced transformation of elastically inactive intrachain cross-linkers to elastically active interchain cross-linkers.

Conclusions

Networks formed from semidilute unentangled solutions of poly(4-vinylpyridine) in DMSO and bis-Pd(II) (or bis-Pt(II)) organometallic cross-linkers are observed to undergo shear thickening above critical rates of steady shear. The shear rates involved in the nonlinear rheological properties scale with the rate of dissociation of the defining metal−ligand bond. Parallel superposition of oscillation onto steady-shear flows facilitates a characterization of the change in network relaxation time from the linear to the shear thickening regime. An increase in the relaxation time is observed, supporting a mechanism in which shear thickening is caused by a shear-induced increase in the number of elastically active chains. The kinetics and magnitude of the shear thickening support this conclusion. An analysis of the different state of cross-linkers further supports that the increased elastically active chains result from the conversion of intrachain cross-linkers to interchain cross-linkers, rather than from dangling state cross-linkers to interchain bound state cross-linkers in our experiments.

Acknowledgment. This work was supported by NSF (CHE-0646670) and NIH (EB-001037). We thank M. Rubinstein for helpful comments.

Supporting Information Available: Characterization of the PVP concentration regime, calculation of the fraction of cross-linker states and activation energies of cross-linker dissociation, and video of the steady shear experiment. This material is available free of charge via the Internet at http://pubs.acs.org.

References and Notes

(1) Reed, A. E.; Curtiss, L. A.; Weinhold, F. *Chem. Rev.* **1988**, *88*, 899–926.
(2) Gans, W.; Boeyens, J. C. A. *Intermolecular Interactions*; Springer: Berlin, 1998.
(3) Larson, R. G. *The Structure and Rheology of Complex Fluids*; Oxford University Press: New York, 1999.
(4) Flory, P. J. *Principles of Polymer Chemistry*; Cornell University Press: Ithaca, NY, 1953.
(5) Rowan, S. J.; Beck, J. B. *Faraday Discuss.* **2005**, *128*, 43–53.
(6) Sijbesma, R. P.; Beijer, F. H.; Brunsveld, L.; Folmer, B. J. B.; Hirschberg, J. H. K.; Lange, R. F. M.; Lowe, J. K. L.; Meijer, E. W. *Science* **1997**, *278*, 1601–1604.
(7) de Greef, T. F. A.; Meijer, E. W. *Nature* **2008**, *453*, 171–173.
(8) Paulusse, J. M. J.; Sijbesma, R. P. *Angew. Chem., Int. Ed.* **2006**, *45*, 2334–2337.
(9) Beck, J. B.; Rowan, S. J. *J. Am. Chem. Soc.* **2003**, *125*, 13922–13923.
(10) Cordier, P.; Tournilhac, F.; Soulie-Ziakovic, C.; Leibler, L. *Nature* **2008**, *451*, 977–980.
(11) Yount, W. C.; Juwarker, H.; Craig, S. L. *J. Am. Chem. Soc.* **2003**, *125*, 15302–15303.
(12) Yount, W. C.; Loveless, D. M.; Craig, S. L. *J. Am. Chem. Soc.* **2005**, *127*, 14488–14496.
(13) Albrecht, M.; van Koten, G. *Angew. Chem., Int. Ed.* **2001**, *40*, 3750–3781.
(14) Serpe, M. J.; Craig, S. L. *Langmuir* **2007**, *23*, 1626–1634.
(15) Loveless, D. M.; Jeon, S. L.; Craig, S. L. *Macromolecules* **2005**, *38*, 10171–10177.
(16) Loveless, D. M.; Abu-Lail, N. I.; Kaholek, M.; Zauscher, S.; Craig, S. L. *Angew. Chem., Int. Ed.* **2006**, *45*, 7812–7814.
(17) Knoben, W.; Besseling, N. A. M.; Cohen Stuart, M. A. *Macromolecules* **2006**, *39*, 2643–2653.
(18) Zhao, Y.; Beck, J. B.; Rowan, S. J.; Jamieson, A. M. *Macromolecules* **2004**, *37*, 3529–3531.
(19) Loveless, D. M.; Jeon, S. L.; Craig, S. L. *J. Mater. Chem.* **2007**, *17*, 56–61.
(20) Terech, P.; Schaffhauser, V.; Maldivi, P.; Guenet, J. M. *Langmuir* **1992**, *8*, 2104–2106.
(21) Shikata, T.; Ogata, D.; Hanabusa, K. *J. Phys. Chem. B* **2004**, *108*, 508–514.
(22) Cates, M. E. *Macromolecules* **1987**, *20*, 2289–2296.
(23) Schwarz, G.; Bodenthin, Y.; Geue, T.; Koetz, J.; Kurth, D. G. *Macromolecules* **2010**, *43*, 494–500.
(24) Hofmeier, H.; Hoogenboom, R.; Wouters, M. E. L.; Schubert, U. S. *J. Am. Chem. Soc.* **2005**, *127*, 2913–2921.
(25) Jeon, S. L.; Loveless, D. M.; Yount, W. C.; Craig, S. L. *Inorg. Chem.* **2006**, *45*, 11060–11068.
(26) Tam, K. C.; Jenkins, R. D.; Winnik, M. A.; Bassett, D. R. *Macromolecules* **1998**, *31*, 4149–4159.
(27) Rubinstein, M.; Semenov, A. N. *Macromolecules* **2001**, *34*, 1058–1068.
(28) Ayyer, R. K.; Leonov, A. I. *Rheol. Acta* **2004**, *43*, 283–292.
(29) Berret, J. F.; Séréro, Y. *Phys. Rev. Lett.* **2001**, *87*, 048303.
(30) Ma, S. X.; Cooper, S. L. *Macromolecules* **2001**, *34*, 3294–3301.
(31) Séréro, Y.; Jacobsen, V.; Berret, J. F.; May, R. *Macromolecules* **2000**, *33*, 1841–1847.
(32) Mewis, J.; Kaffashi, B.; Vermant, J.; Butera, R. J. *Macromolecules* **2001**, *34*, 1376–1383.
(33) Tripathi, A.; Tam, K. C.; McKinley, G. H. *Macromolecules* **2006**, *39*, 1981–1999.
(34) Tan, H.; Tam, K. C.; Jenkins, R. D. *Langmuir* **2000**, *16*, 5600–5606.
(35) Berret, J. F.; Séréro, Y.; Winkelman, B.; Calvet, D.; Collet, A.; Viguier, M. *J. Rheol.* **2001**, *45*, 477–492.
(36) Ballard, M. J.; Buscall, R.; Waite, F. A. *Polymer* **1988**, *29*, 1287–1293.
(37) Indei, T.; Koga, T.; Tanaka, F. *Macromol. Rapid Commun.* **2005**, *26*, 701–706.
(38) Marrucci, G.; Bhargava, S.; Cooper, S. L. *Macromolecules* **1993**, *26*, 6483–6488.

(39) Indei, T. *J. Non-Newtonian Fluid Mech.* **2007**, *141*, 18–42.
(40) Regalado, E. J.; Selb, J.; Candau, F. *Macromolecules* **1999**, *32*, 8580–8588.
(41) Wang, S. Q. *Macromolecules* **1992**, *25*, 7003–7010.
(42) Witten J, T. A.; Cohen, M. H. *Macromolecules* **1985**, *18*, 1915–1918.
(43) Kersey, F. R.; Yount, W. C.; Craig, S. L. *J. Am. Chem. Soc.* **2006**, *128*, 3886–3887.
(44) Vermant, J.; Walker, L.; Moldenaers, P.; Mewis, J. *J. Non-Newtonian Fluid Mech.* **1998**, *79*, 173–189.
(45) Tirtaatmadja, V.; Tam, K. C.; Jenkins, R. D. *Macromolecules* **1997**, *30*, 1426–1433.
(46) Munoz, M. E.; Santamaría, A.; Guzmán, J.; Riande, E. *J. Rheol.* **2003**, *47*, 1041–1050.
(47) Rubinstein, M.; Colby, R. H. *Polymer Physics*; Oxford University Press: New York, 2003.
(48) Vaccaro, A.; Marrucci, G. *J. Non-Newtonian Fluid Mech.* **2000**, *92*, 261–273.
(49) Anslyn, E. V.; Dougherty, D. A. *Modern Physical Organic Chemistry*; University Science: Mill Valley, CA , 2005.